ChemComm

Chemical Communications

www.rsc.org/chemcomm

Volume 48 | Number 9 | 30 January 2012 | Pages 1185–1324

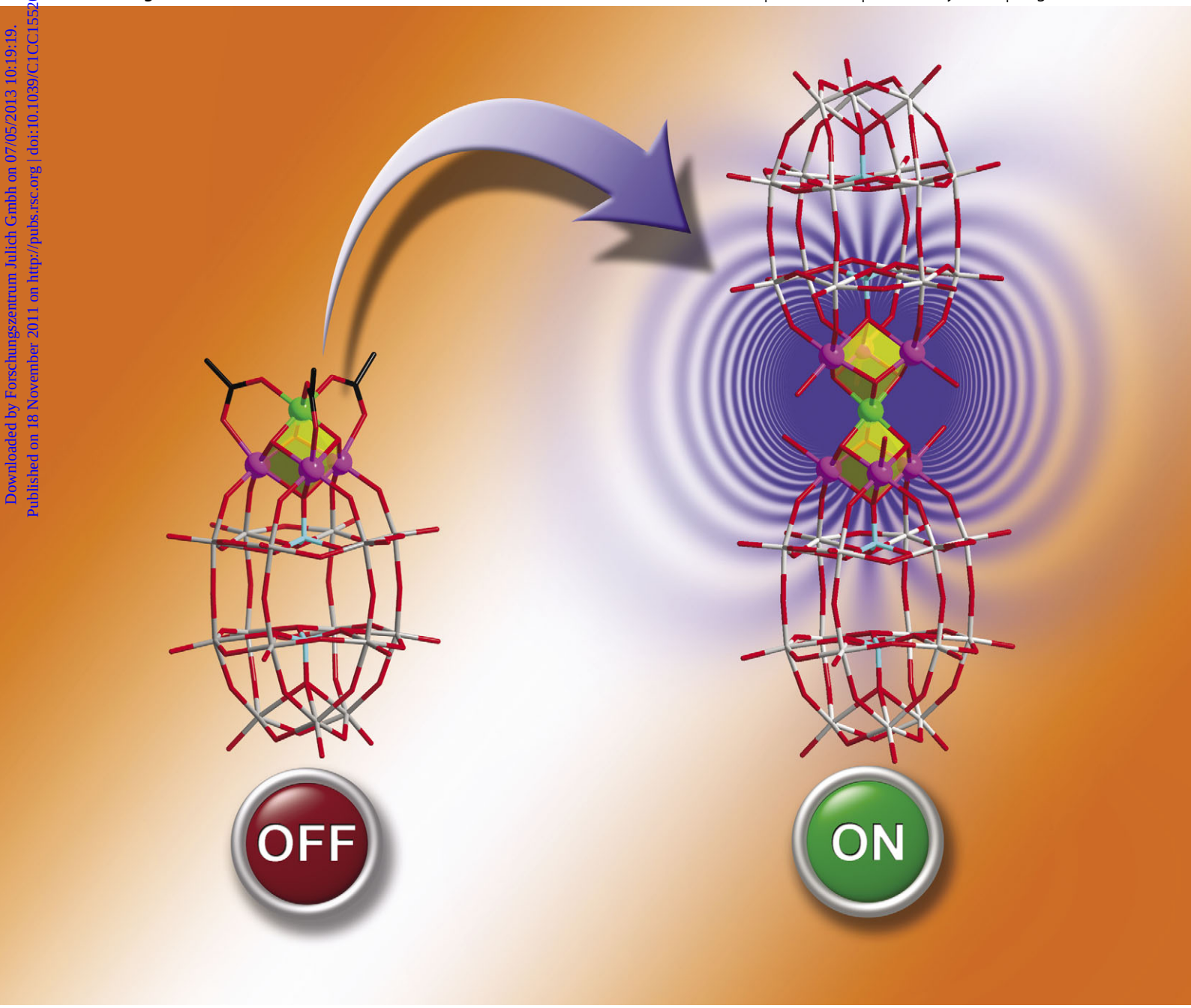

ISSN 1359-7345

RSC Publishing

COMMUNICATION

Fang and Kögerler *et al.*

A polyoxometalate-based single-molecule magnet with an $S = 21/2$ ground state

1359-7345(2012)48:9;1-3

ChemComm

Dynamic Article Links
View Article Online

Cite this: *Chem. Commun.*, 2012, **48**, 1218–1220

www.rsc.org/chemcomm

COMMUNICATION

A polyoxometalate-based single-molecule magnet with an $S = 21/2$ ground state†

Xikui Fang,*[a] Paul Kögerler,*[b] Manfred Speldrich,[b] Helmut Schilder[b] and Marshall Luban[a]

Received 6th September 2011, Accepted 28th October 2011
DOI: 10.1039/c1cc15520b

Ligand modification transforms a polyoxometalate-anchored cubane-type $[Mn^{III}_3Mn^{IV}O_4]$ core into a centrosymmetric $[Mn^{III}_6Mn^{IV}O_8]$ di-cubane cluster, and restores the slow magnetization relaxation characteristics typical for $[Mn_4O_4]$ cubane-based single-molecule magnets.

For almost two decades since the discovery of single-molecule magnet (SMM) phenomena in transition-metal coordination clusters,[1] the development of new SMMs has largely made use of organic supporting ligands, for example, carboxylates, alkoxides, and amines. Despite a continuous stream of magnetic molecules featuring diverse metal ions, nuclearities, and topologies,[2] little progress has been made[3] in achieving a significant increase in the blocking temperature (below which magnetic hysteresis becomes evident) for such organic-bridged SMMs. The inherent flexibility of many organic ligands makes it difficult to restrain the alignment of spin centers and regulate intramolecular exchange coupling. More rigorous synthetic control, thus, calls for supporting ligands of less flexibility.

Inorganic polyoxometalates[4] (POMs) fit this requirement: their well-defined, rigid coordination environments can in principle facilitate targeted design of magnetic core structures. Polyoxoanion ligands have also been found to induce strong axial magnetic anisotropy, illustrated by a Mn^{II}–POM complex.[5] An additional advantage stems from the limited intermolecular interactions between POMs, separated by counterions and solvent, which can lead to increased isolation of the ground state. In recent years, a handful of POM-based SMMs,[6] with ground state spins as high as $S = 8$,[6f] have been assembled from lacunary polyoxoanion ligands and one or more open-shell metal atoms, typically starting from simple salts of 3d and 4f ions as precursors. We have been taking a different synthetic approach, namely, replacing organic bridging groups on preformed metal-carboxylate clusters with POM ligands.[7–10] This strategy thus offers a greater degree of control over core structures and their spin states, as demonstrated here in the construction of a heptanuclear manganese cluster with a record $S = 21/2$ ground multiplet for POM-based SMMs. The result also suggests the important consequence of molecular symmetry and electric dipole moment on the magnetic properties of this cluster.

The story starts with a tetranuclear $[Mn^{III}_3Mn^{IV}O_4]$ cubane cluster[8] that we recently obtained from reaction of the prototypical SMM Mn_{12}-acetate[11] with $[\alpha\text{-}P_2W_{15}O_{56}]^{12-}$, a diamagnetic polyoxotungstate. The magnetic core of the resulting complex $[(\alpha\text{-}P_2W_{15}O_{56})Mn^{III}_3Mn^{IV}O_3(CH_3COO)_3]^{8-}$ (**1**), shown in Fig. 1 (left), is supported by the heptadentate $\{P_2W_{15}\}$ ligand and reinforced with three capping acetate groups. Like other organic-bridged $\{Mn^{III}_3Mn^{IV}\}$ SMMs of the cubane type,[2,12] **1** displays an $S = 9/2$ spin ground state arising from antiferromagnetic exchange between a Mn^{IV} ($S = 3/2$) apex and a triangle of three ferromagnetically coupled Mn^{III} ($S = 2$) ions. However, **1** does not constitute an SMM, which we attribute to a positive axial anisotropy ($D = +0.36\ cm^{-1}$) that leads to

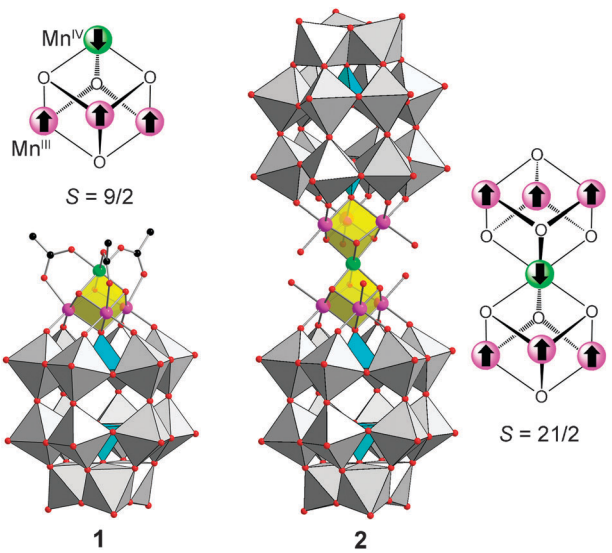

Fig. 1 Ball-and-stick/polyhedral representations of polyoxoanion complexes **1** and **2** with their magnetic core structures highlighted in yellow. Proposed ground state spin alignments are shown in separate schematic diagrams. Mn^{IV}: green; Mn^{III}: purple; O: red; C: black; WO_6: gray octahedra; PO_4: blue tetrahedra.

[a] *Ames Laboratory, US DOE and Department of Physics and Astronomy, Iowa State University, Ames, IA 50011, USA. E-mail: xfang@ameslab.gov; Fax: +1 515-294-0689; Tel: +1 515-294-7505*
[b] *Institute of Inorganic Chemistry, RWTH Aachen University, D-52074 Aachen, Germany. E-mail: paul.koegerler@ac.rwth-aachen.de; Fax: +49 241 8092642*

† Electronic supplementary information (ESI) available: Synthesis and characterization data of **2a**. CSD 423436. CCDC 843427. For ESI and crystallographic data in CIF or other electronic format see DOI: 10.1039/c1cc15520b

a reverse order of the zero-field split substates and thus an absence of slow magnetization relaxation.[8]

With this high-spin molecule at hand, we now aim to enhance the spin ground state and magnetic anisotropy of compound **1** *via* ligand modification. Herein we derive a closely related Mn_7 POM cluster, whereby the ground state spin is significantly increased and SMM behavior, in particular slow magnetization relaxation, is indeed observed. To realize higher spin states, we initially intended to induce further growth of the magnetic core by removing the acetate bridges, as they essentially terminate the coordination sphere of the Mn centers. Efforts to directly expand from compound **1**, employed as a precursor, however did not succeed, suggesting the importance of acetate bridges to the stability of the Mn_4 core. Ligand change is eventually achieved by adapting the synthesis of **1** but using water as the solvent instead of a 3 : 2 (v/v) mixture of CH_3COOH/H_2O, from which compound **1** is isolated.‡ This *in situ* method effectively prevents the formation of acetate bridges, resulting in an all-inorganic cluster $[(\alpha\text{-}P_2W_{15}O_{56})_2Mn^{III}{}_6Mn^{IV}O_6(H_2O)_6]^{14-}$ (**2**, Fig. 1, right) as its sodium salt $Na_{14}\mathbf{2}\cdot 68H_2O$ (**2a**).§

The structure of **2** is composed of two units of $\{P_2W_{15}\}$ that encapsulate a heptanuclear $[Mn^{III}{}_6Mn^{IV}O_8]$ core.[13] The Mn_7 core resembles two corner-sharing cubanes such that it can be formally constructed from the fusion of two Mn_4 cores to share a common Mn^{IV} vertex. The bridging acetate groups in **1** are now replaced with terminal aqua ligands, the latter completing the octahedral geometry of the Jahn–Teller (JT) distorted (tetragonally elongated) Mn^{III} centers and defining the orientation of their elongation axes. The angles between the JT axes and the C_3 axis of the molecule, avg. 54.59°, deviate minimally from those of compound **1** (avg. 56.36°). The removal of acetate bridges between Mn^{III} and Mn^{IV} ions has also resulted in slightly longer $Mn^{III}\cdots Mn^{IV}$ distances (avg. 2.855 *vs.* 2.801 Å in **1**) and a concomitant decrease in $Mn^{III}\cdots Mn^{III}$ distances (avg. 3.092 *vs.* 3.152 Å). Overall, anion **2** has approximate D_{3d} symmetry with the Mn^{IV} ion at the inversion center. Given the structural similarity in magnetic cores of the two structures, one would expect the exchange couplings between the Mn ions to remain ferromagnetic for Mn^{III}–Mn^{III} and antiferromagnetic for Mn^{III}–Mn^{IV} interactions. That would align the spins of the six Mn^{III} atoms all parallel, and antiparallel to the central Mn^{IV} atom, predicting a molecular $S = 21/2$ ground state in a spin-only approximation.

Results from magnetic measurements support this prediction. The value of $\chi_m T$ at 290 K (30.0 emu K mol^{-1}) is significantly higher than the spin-only value (19.875 emu K mol^{-1}, $g = 2.0$) for six Mn^{III} and one Mn^{IV} non-coupled ions, indicative of ferromagnetic interaction (Fig. 2a). Upon cooling, the value of $\chi_m T$ gradually increases to a maximum of 59.7 emu K mol^{-1}, followed by a sudden decrease at 5 K. The maximum value is comparable with the spin-only value of 60.375 emu K mol^{-1} for an $S = 21/2$ state. Based on the approximate D_{3d} point group symmetry of **2**, the exchange interactions are grouped in Mn^{III}–Mn^{IV} (J_1) and Mn^{III}–Mn^{III} (J_2) contacts, each mediated by two μ-O sites:

$$H_{ex} = -2\left[\begin{array}{l} J_1(\hat{S}_1\cdot\hat{S}_2+\hat{S}_1\cdot\hat{S}_3+\hat{S}_1\cdot\hat{S}_4+\hat{S}_1\cdot\hat{S}_5+\hat{S}_1\cdot\hat{S}_6+\hat{S}_1\cdot\hat{S}_7)+ \\ J_2(\hat{S}_2\cdot\hat{S}_3+\hat{S}_3\cdot\hat{S}_4+\hat{S}_4\cdot\hat{S}_2+\hat{S}_5\cdot\hat{S}_6+\hat{S}_6\cdot\hat{S}_7+\hat{S}_7\cdot\hat{S}_5) \end{array}\right]$$

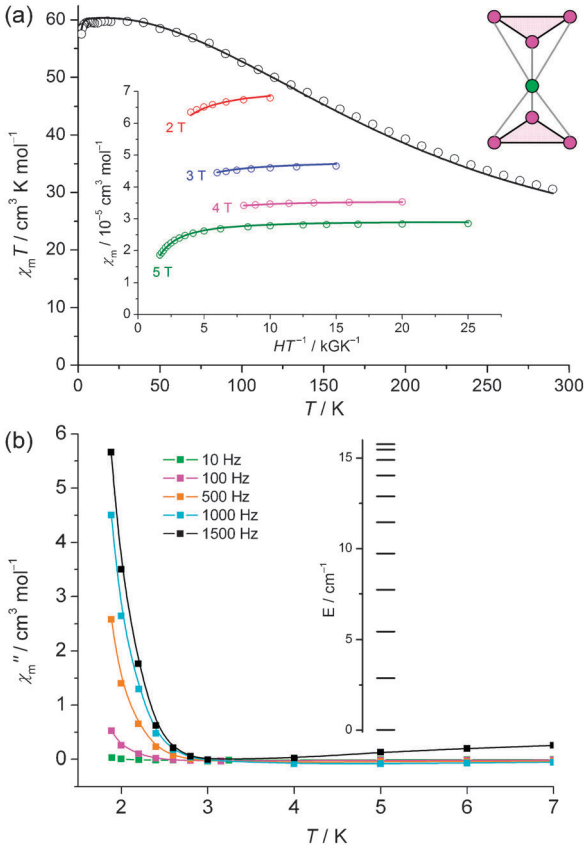

Fig. 2 Magnetic data for **2a**. (a) Temperature and field-dependence of $\chi_m T$ ($B = 0.1$ T) and χ_m (inset). Circles: experimental data; graphs: least-squares fit (see text). The $\{Mn_7\}$ exchange coupling scheme (right) illustrates the underlying 2-J model of one Mn^{IV} center (green) sandwiched between two equilateral $Mn^{III}{}_3$ triangles (pink). Grey lines represent J_1; black lines J_2. (b) Temperature dependence of the out-of-phase susceptibility contribution χ_m'' ($H_{dc} = 0$). Inset: Zero-field splitting of the ground state multiplet resulting from CONDON simulations.

Furthermore, the deviation from isotropic Brillouin-type field-dependent magnetization curves at low temperatures (T = 1.8–5 K; Fig. 2a, inset) indicates strong zero-field splitting of the Mn^{III} centers in their JT-elongated octahedral environments ($^5B_{1g}$), whereas the Mn^{IV} center represents an isotropic spin-3/2 site ($^4A_2$). Therefore, an accurate magnetochemical interpretation of the $\{Mn^{III}{}_6Mn^{IV}\}$ spin polytope in **2** relies on modeling all relevant single-ion effects as well as Heisenberg-type exchange coupling. The Hamiltonian is implemented in the computational framework CONDON,[14] which takes into account the full d manifolds. The computational key requirement is the identification of a sufficiently large energy gap relative to the maximum temperatures of the experimental data so that higher states can be discarded without any significant effect on the magnetic properties at lower temperatures. Simultaneous fitting to temperature- and field-dependent susceptibility data confirms the $S = 21/2$ ground state and results in near-perfect fits under consideration of the single ion effects, while the basis was adjusted to accommodate the resulting matrices within the available memory (96 gigabytes). Refining the ligand field parameters (B_0^k values, see ESI†)[15] and J_1 and J_2 by a least-squares fit fully reproduces all data (SQ = 1.98%) and yields $B_0^2 = -5370$ cm^{-1}, $B_0^4 = 17\,180$ cm^{-1}, $B_4^4 = 1850$ cm^{-1},

$J_1 = -18.75\ cm^{-1}$, and $J_2 = 12.5\ cm^{-1}$. The signs of the refined B_q^k values agree with PCEM results and are in line with the ligand fields found for compound **1**.[8] However, the two types of Mn–Mn exchange interactions respond very differently to the removal of acetate bridges, despite that all these distances are comparable to those in **1**. The magnitude of Mn^{III}–Mn^{III} coupling (J_2) is little changed (*vs.* 10.2 cm^{-1} in **1**) whereas the Mn^{III}–Mn^{IV} coupling (J_1) is considerably weakened (*vs.* $-31.3\ cm^{-1}$), again indicating the significant influence of acetate superexchange pathways.

Compared to the static magnetic data, frequency-dependent ac susceptibility results (Fig. 2b) are characteristic of a SMM, where (in a pure-spin approximation) the m_S substates of the $S = 21/2$ ground state multiplet are zero-field-split to result in a parabolic energy barrier between the highest $\pm m_S$ ($\pm 21/2$) substates causing a slowing of the magnetization relaxation upon a field change. For **2**, the total zero-field splitting of 15.7 cm^{-1} of the ground state derived from CONDON results (Fig. 2b, inset) relates to the empirical parameter $D = -0.143\ cm^{-1}$. An out-of-phase (χ'') component of the ac susceptibility emerges below 3 K, however a fit to a (phenomenological) Arrhenius expression in order to establish the effective energy barrier U_{eff} fails as no maxima in χ'' are observed within the experimental limits. Likewise, a fitting attempt using a generalized Debye model[16] does not yield maxima in the χ'' *vs.* χ' Cole–Cole representation even for the temperatures and angular frequencies experimentally available.

We note that the existence of an energy barrier of the zero-field-split ground state evident from the ac susceptibility is in stark contrast to compound **1** in which a single $\{Mn^{III}{}_3Mn^{IV}O_4(CH_3COO)_3\}$ cubane group is directly coordinated to a $\{P_2W_{15}\}$ group.[8] Here, the $\{Mn^{III}{}_3Mn^{IV}O_4\}$ substructure—a crucial feature of numerous $S = 9/2$ SMMs—is characterized by an "inverted" parabola of m_S substates, leaving the $m_S = \pm 1/2$ substates the energetically lowest. Comparing these results to compound **2**, where the geometric parameters relevant to the molecular magnetic anisotropy (*e.g.* the alignment between the JT axes) are very similar, we tentatively attribute this unexpected sign change in D to the pronounced dipole moment of **1** *vs.* the absence of a dipole moment in **2**. The underlying electrical field caused by the $[Mn^{III}{}_3Mn^{IV}O_4(CH_3COO)_3]^{2+}$ group and $[P_2W_{15}O_{55}]^{10-}$ likely influences the spin–orbit coupling which fundamentally depends on the electrical field gradient.[17] As spin–orbit coupling in turn also influences the zero-field splitting, the energy barrier between m_S states is affected, too. Correspondingly, the absence of a significant net dipole moment in **2**, as well as in all other published polyoxometalate-based SMMs, appears to preserve the energy barrier originating from zero field-splitting.

We are grateful to Dr Gordon Miller for allowing us access to X-ray facilities. Ames Laboratory is operated for the U.S. Department of Energy by Iowa State University under Contract No. DE-AC02–07CH11358.

Notes and references

‡ Synthesis of **2a**: a sample of $[Mn^{III}{}_8Mn^{IV}{}_4O_{12}(CH_3COO)_{16}(H_2O)_4]\cdot 4H_2O\cdot 2CH_3COOH$ (0.15 g, 0.07 mmol) was suspended in H_2O (20 mL). Solid $Na_{12}[\alpha\text{-}P_2W_{15}O_{56}]\cdot 18H_2O$ (0.5 g, 0.12 mmol) was added to the mixture in small portions over a period of 10 min with vigorous stirring. After stirring for 0.5 h at room temperature, the mixture was heated to 80 °C for another 1.5 h and hot filtered. Solid NaCl (0.6 g) was then added to the filtrate. Dark red crystals of **2a** (stacked plates) were collected from the solution after 2–3 weeks of slow evaporation, with a yield of 70 mg (12.6% based on W). See ESI† for experimental details.

§ Crystal data for **2a**: $H_{148}Mn_7Na_{14}O_{192}P_4W_{30}$, $M = 9567.00\ g\ mol^{-1}$, space group $P\bar{1}$, $a = 12.700(4)$, $b = 15.684(5)$, $c = 22.216(7)$ Å, $\alpha = 97.549(5)°$, $\beta = 95.210(5)°$, $\gamma = 103.775(5)°$, $V = 4226(2)$ Å^3, $T = 173(2)$ K, $Z = 1$, $D_c = 3.759\ Mg\ m^{-3}$, $F(000) = 4293$, μ(Mo-Kα) = 21.029 mm^{-1}. 45 297 reflections measured, 17 111 unique ($R_{int} = 0.0426$). The refinement converges to $R_1 = 0.0637$, w$R_2 = 0.1474$ and GOF = 1.033 for 13 834 reflections with $I > 2\sigma(I)$. CSD 423436.

1 (*a*) R. Sessoli, H. L. Tsai, A. R. Schake, S. Y. Wang, J. B. Vincent, K. Folting, D. Gatteschi, G. Christou and D. N. Hendrickson, *J. Am. Chem. Soc.*, 1993, **115**, 1804; (*b*) R. Sessoli, D. Gatteschi, A. Caneschi and M. A. Novak, *Nature*, 1993, **365**, 141.

2 (*a*) D. Gatteschi, R. Sessoli and J. Villain, *Molecular Nanomagnets*, Oxford University Press, Oxford, 2006; (*b*) G. Aromí and E. K. Brechin, *Struct. Bonding*, 2006, **122**, 1.

3 (*a*) J. D. Rinehart, M. Fang, W. J. Evans and J. R. Long, *Nat. Chem.*, 2011, **3**, 538 and references therein; (*b*) C. J. Milios, A. Vinslava, W. Wernsdorfer, S. Moggach, S. Parsons, S. P. Perlepes, G. Christou and E. K. Brechin, *J. Am. Chem. Soc.*, 2007, **129**, 2754; (*c*) R. Inglis, J. Bendix, T. Brock-Nannestad, H. Weihe, E. K. Brechin and S. Piligkos, *Chem. Sci.*, 2010, **1**, 631.

4 (*a*) *Polyoxometalates: from Platonic Solids to Anti-Retroviral Activity*, ed. M. T. Pope and A. Müller, Kluwer Academic Publishers, Dordrecht, 1994; (*b*) Topical issue on polyoxometalates: C. L. Hill (guest ed.), *Chem. Rev.*, 1998, **98**, 1; (*c*) A. Proust, R. Thouvenot and P. Gouzerh, *Chem. Commun.*, 2008, 1837; (*d*) A. Dolbecq, E. Dumas, C. R. Mayer and P. Mialane, *Chem. Rev.*, 2010, **110**, 6009.

5 C. Pichon, P. Mialane, E. Rivière, G. Blain, A. Dolbecq, J. Marrot, F. Sécheresse and C. Duboc, *Inorg. Chem.*, 2007, **46**, 7710.

6 (*a*) C. Ritchie, A. Ferguson, H. Nojiri, H. N. Miras, Y.-F. Song, D.-L. Long, E. Burkholder, M. Murrie, P. Kögerler, E. K. Brechin and L. Cronin, *Angew. Chem., Int. Ed.*, 2008, **47**, 5609; (*b*) M. A. AlDamen, J. M. Clemente-Juan, E. Coronado, C. Marti-Gastaldo and A. Gaita-Arino, *J. Am. Chem. Soc.*, 2008, **130**, 8874; (*c*) J. Compain, P. Mialane, A. Dolbecq, I. M. Mbomekalle, J. Marrot, F. Secheresse, E. Riviere, G. Rogez and W. Wernsdorfer, *Angew. Chem., Int. Ed.*, 2009, **48**, 3077; (*d*) A. Giusti, G. Charron, S. Mazerat, J.-D. Compain, P. Mialane, A. Dolbecq, E. Rivière, W. Wernsdorfer, R. N. Biboum, B. Keita, L. Nadjo, A. Filoramo, J.-P. Bourgoin and T. Mallah, *Angew. Chem., Int. Ed.*, 2009, **48**, 4949; (*e*) M. A. AlDamen, S. Cardona-Serra, J. M. Clemente-Juan, E. Coronado, A. Gaita-Arino, C. Marti-Gastaldo, F. Luis and O. Montero, *Inorg. Chem.*, 2009, **131**, 12558; (*f*) M. Ibrahim, Y. Lan, B. S. Bassil, Y. Xiang, A. Suchopar, A. K. Powell and U. Kortz, *Angew. Chem., Int. Ed.*, 2011, **50**, 4708; (*g*) C. Ritchie, M. Speldrich, R. W. Gable, L. Sorace, P. Kögerler and C. Boskovic, *Inorg. Chem.*, 2011, **50**, 7004.

7 X. Fang and M. Luban, *Chem. Commun.*, 2011, **47**, 3066.

8 X. Fang, M. Speldrich, H. Schilder, R. Cao, K. P. O'Halloran, C. L. Hill and P. Kögerler, *Chem. Commun.*, 2010, **46**, 2760.

9 X. Fang and P. Kögerler, *Angew. Chem., Int. Ed.*, 2008, **47**, 8123.

10 X. Fang and P. Kögerler, *Chem. Commun.*, 2008, 3396.

11 T. Lis, *Acta Crystallogr., Sect. B: Struct. Crystallogr. Cryst. Chem.*, 1980, **36**, 2042.

12 S. M. J. Aubin, M. W. Wemple, D. M. Adams, H.-L. Tsai, G. Christou and D. N. Hendrickson, *J. Am. Chem. Soc.*, 1996, **118**, 7746, and references therein.

13 The oxidation states of Mn centers are determined from bond valence calculations (Mn^{III}, 2.95–2.98; Mn^{IV}, 3.90) and also based on the characteristic Jahn–Teller distortion for Mn^{III} (HS d^4).

14 M. Speldrich, H. Schilder, H. Lueken and P. Kögerler, *Isr. J. Chem.*, 2011, **51**, 215.

15 (*a*) C. Görller-Walrand and K. Binnemans, in *Handbook on the Physics and Chemistry of Rare Earths*, ed. K. A. Gschneidner, Jr. and L. Eyring, Elsevier, Amsterdam, 1996, vol. 23, pp. 121–283; (*b*) B. G. Wybourne, *Spectroscopic Properties of Rare Earths*, Wiley, New York, 1965.

16 K. S. Cole and R. H. Cole, *J. Chem. Phys.*, 1941, **9**, 341.

17 A. Messiah, *Quantum Mechanics*, Dover Publications, Mineola, 1999, vol. 2, ch. 20.